# 基于曲率传感的稀疏孔径望远镜共焦检测方法研究

安其昌[1,2], 吴小霞[1,2], 李洪文[1,2]

(1. 中国科学院长春光学精密机械与物理研究所, 吉林 长春 130033;
2. 吉林省智能波前传感与控制重点实验室, 吉林 长春 130033)

**摘 要:** 为了更好地对大口径稀疏孔径望远镜进行共焦调控,利用曲率传感方法非干涉、大范围、波段鲁棒的特点。首先,利用近场电磁波的传输方程分析了稀疏孔径望远镜共焦调控的基本原理。其次,结合曲率传感理论,进行了稀疏孔径望远镜共焦调控误差分析。再次,对于曲率传感稀疏孔径望远镜共焦检测的可行性进行了分析与实验。之后,利用桌面实验实现了大口径稀疏孔径望远镜共焦检测的原理贯通。最终,波前倾斜探测结果与原始波前相比,相关性从 0.26 上升至 0.83。利用曲率传感可实现 20 个波长范围的共焦测量,避免了传统方法对像点进行多次移动标校以及逐个调节的缺点。文中实现了大通量共焦误差感知与收敛调控,为未来大口径稀疏孔径望远镜的建设打下技术基础。

**关键词:** 曲率传感; 波前像差; 稀疏孔径望远镜; 共焦

**中图分类号:** TH751 **文献标志码:** A **DOI:** 10.3788/IRLA20230050

## 0 引 言

为追求更大的集光面积与探测灵敏度,未来望远镜的口径越来越大[1]。大口径稀疏孔径望远镜是未来建设超大口径望远镜重要的技术路线之一,目前最大口径的稀疏孔径望远镜为大麦哲伦望远镜 (24 m),已完成了多块主镜的加工。针对大口径稀疏孔径望远镜,需要将多块子镜的指向集中于一点,即共焦[2−5]。

针对稀疏孔径的共焦 (光轴对准) 是实现望远镜既定科学目标的基础,同时,也是将多路系统实现功能合成的关键。盖亚巡天望远镜离轴主镜 1.46 m×0.51 m,焦面探测器由 106 块 CCD 拼接而成,同时系统具有两台相对独立的望远镜。两台望远镜共用第五镜、第六镜以及焦面探测器,采用哈特曼进行波前拼接传感,共焦精度优于两个像素[6]。

目前,研究空间望远镜集成定标的前沿团队为美国国家航空航天局开发的空间望远镜詹姆斯·韦布望远镜团队。为了实现望远镜中 132 个自由度的校准,该团队采用三个 1.5 m 的均布离散孔径,对口径为 6.5 m 的系统波前进行检测,深入研究了系统像差解算与系统失调量估计[7]。国内方面,大天空区域多目标光纤光谱望远镜利用哈特曼波前传感器进行共焦测量,保证所有子镜的能量进行重叠[8]。中国科学院云南天文台的刘忠等在环形太阳望远镜计划的研究中,利用斜率计对环形望远镜的共焦进行辅助测量[9]。

共焦探测所需波前传感动态范围要求较大[10]。对于哈特曼传感器而言,可采用大口径的子孔径提升动态范围,但会导致子孔径中加入其他像差成分,偏离高斯假设。目前的波前传感方法主要面临两方面的限制,即大动态范围的波前传感架构,对于像差校正残差的灵敏度较低,无法进一步提升波前的校正精度,对于精细天文观测等应用场景均会有巨大的限制。同时,过大的动态范围会导致解算非线性加剧,引起波前校正系统的控制性能退化。不仅如此,宽带探测具有灵敏度高、结构简单的特点,在盖亚巡天望远镜、中国空间站巡天望远镜等大规模巡天,以及大麦哲伦望远镜[2]、30 m 望远镜[11],欧洲极大口径望远镜[12] 等下一代通用大口径望远镜中都有重要的应用,

**收稿日期:** 2023−02−06; **修订日期:** 2023−04−13

**基金项目:** 国家自然科学基金项目 (12133009, 12373090); 中国科学院青年创新促进会项目 (2020221);
中国科学院关键核心技术攻关项目 (YZQT024)

**作者简介:** 安其昌,男,副研究员,博士,主要研究方向为大口径光机系统检测装调。

为实现宽带观测下的共焦测试，也要求波前传感方法具有对波长的鲁棒性。针对稀疏孔径望远镜所有子镜像点均进入探测器后的共焦过程，在此采用了曲率传感实现大范围的波前感知 (利用系统焦面，不需要额外光路，不引入非公共光路像差)，以提升多个子镜像点聚焦于统一位置的精度与速度。

## 1 曲率传感基本原理

对焦前焦后 (利用调焦机构等方法) 的两组图像强度进行差分，对波前的曲率进行估计。通过感知大口径稀疏孔径望远镜子镜间倾斜所造成的局部曲率变化，并通过对子镜区域进行平面拟合实现倾斜感知，具体如图 1 所示。

根据近场电磁波的传输方程[13] 可以解算出波前信息，如公式 (1) 所示：

$$\frac{\partial I(\vec{\rho})}{\partial z}=-\left(\delta(\vec{\rho})\nabla\Phi(\vec{\rho})+I(\vec{\rho})\nabla^2\Phi(\vec{\rho})\right) \tag{1}$$

式中：$I(\vec{\rho})$为强度；$\Phi(\vec{\rho})$为相位；$\nabla$为梯度算子，得到的结果为斜率；$\nabla^2$为拉普拉斯算子，得到的结果为曲率；$\vec{\rho}$为光瞳内坐标；$\delta$为狄拉克函数。可见，其结果与子镜边界的变化直接相关。

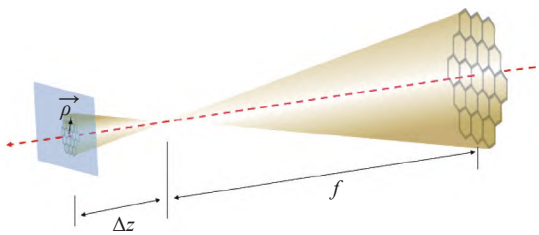


图 1 曲率传感原理图

Fig.1 Schematic diagram of curvature sensing

## 2 曲率传感共焦检测精度分析

大口径稀疏孔径望远镜共焦测量主要分为利用焦面与瞳面两种方式。瞳面方法具有代表性的为詹姆斯韦布望远镜，通过光瞳相机对最终系统的对准情况进行校验[14]。光瞳方法动态范围较小，仅在理想位置附近才能形成清晰的光瞳像。同时，需要光瞳共轭光路，对靶面大小的要求较高。焦面方法具有精度高、动态范围大、相机尺寸要求低的优点，在詹姆斯韦布望远镜中也采用了焦面方式作为前置的调控环节。但需要先对各个光点进行分辨与逐个调节，感知效率较低，严重影响系统调控带宽。

首先，获得焦前焦后两幅离焦星点像，基于波前曲率传感方法通过离焦星点像实现解算波前。之后，利用掩模版对星点像边缘噪声进行抑制，即利用波前边界假设对波前迭代过程进行物理约束。在此基础上，通过平面拟合可实现共焦感知与调控。基于曲率传感的稀疏孔径望远镜共焦检测方法如图 2 所示，克服了传统方法光点重叠后便会丢失、需要重新定标的缺点。

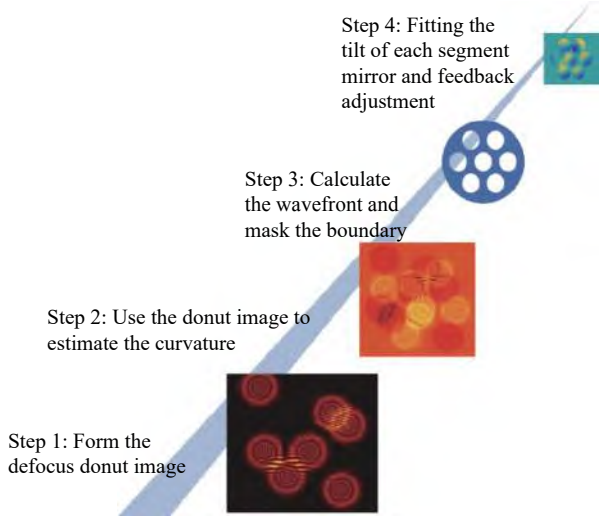


图 2 基于曲率传感的稀疏孔径望远镜共焦检测方法

Fig.2 Co-focus detection method of sparse aperture telescope based on curvature sensing

基于以上方法，针对大幅值波前倾斜，即系统初始失调严重情况感知效果如图 3 所示。小幅值波前倾斜，即系统接近对准情况感知效果如图 4 所示。可见，该方法可在不进行焦点识别的前提下实现对多个镜面倾斜的并行感知与调控。

单一口径的望远镜在热载荷作用下，产生的误差以球差为主，其最基本的特征为镜面的“最接近球面”发生了变化 (即曲率变化)，而对于大口径稀疏孔径望远镜每个单镜受到热载荷影响的同时，会产生整体“离焦模式”。在此模式下，边缘传感器无法通过子镜边缘高度的变化判断其行为模式，导致系统的可控性下降。因此，需要利用波前传感调节系统的大范围离焦与球差后，再进行子镜的倾斜校正。子镜整体低阶像差感知与调控过程如图 5 所示。

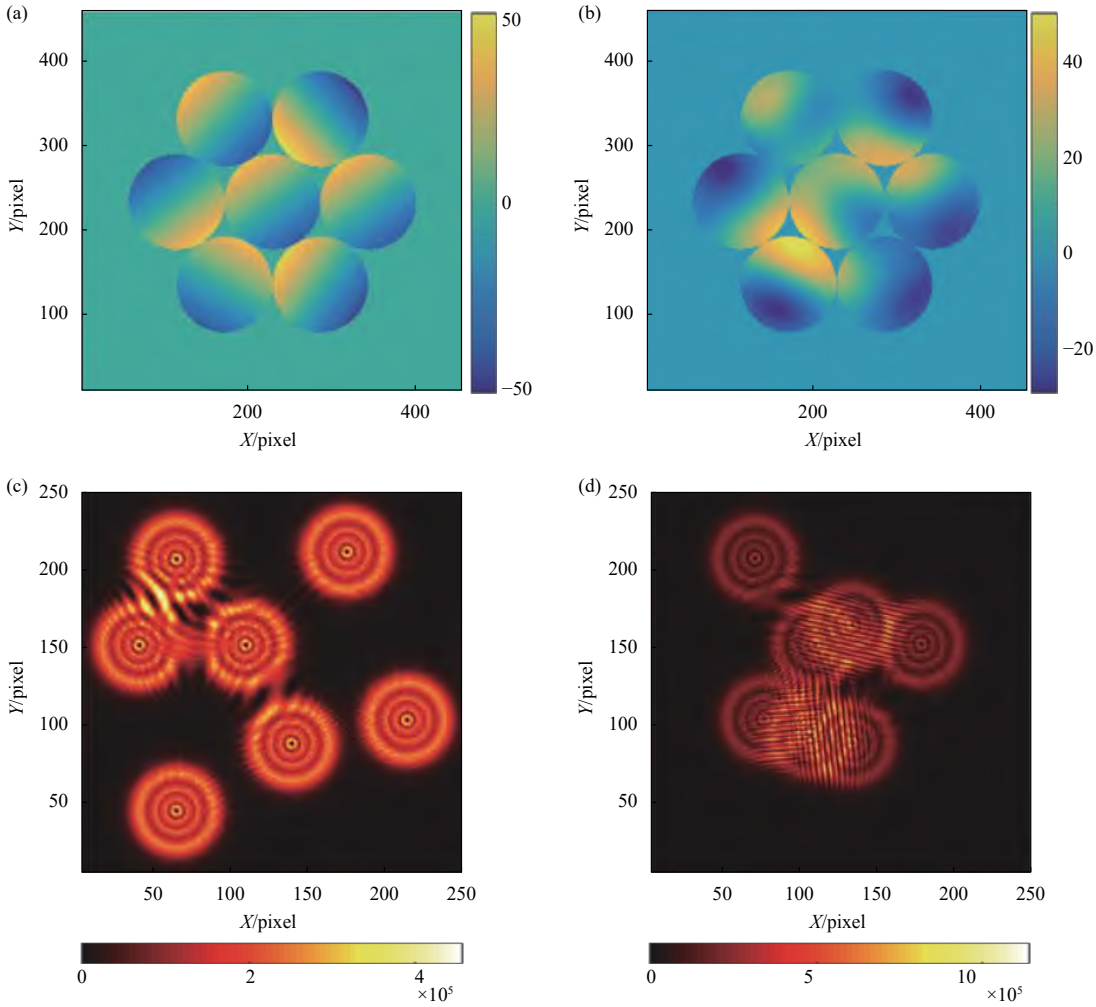


图 3 大幅值波前倾斜感知效果。(a) 倾斜波前; (b) 重建波前; (c) 焦前光强分布; (d) 焦后光强分布

Fig.3 Large amplitude wavefront tilt sensing. (a) Tilt wavefront; (b) Reconstruction wavefront; (c) Intensity distribution before focus; (d) Intensity distribution after focus

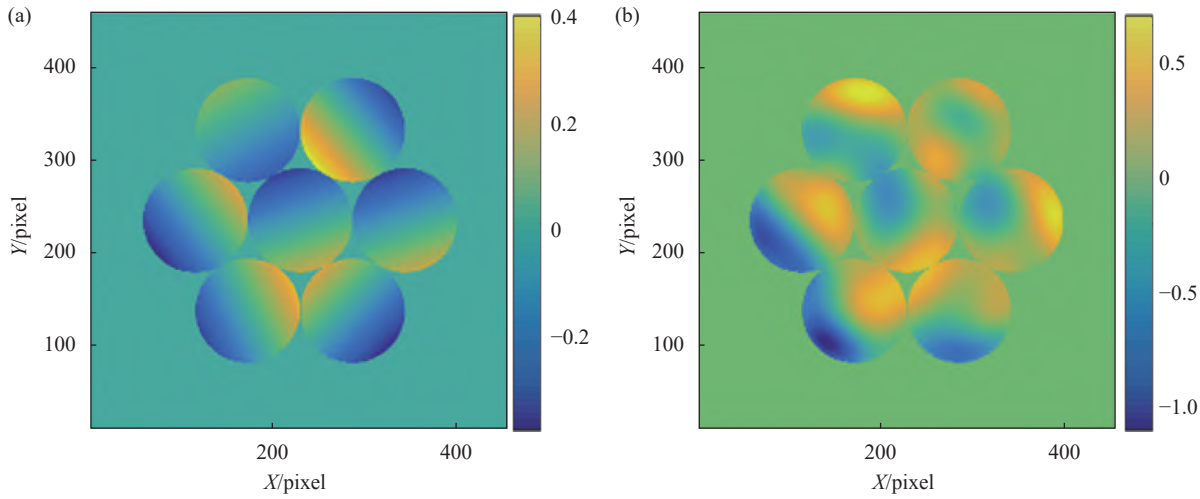

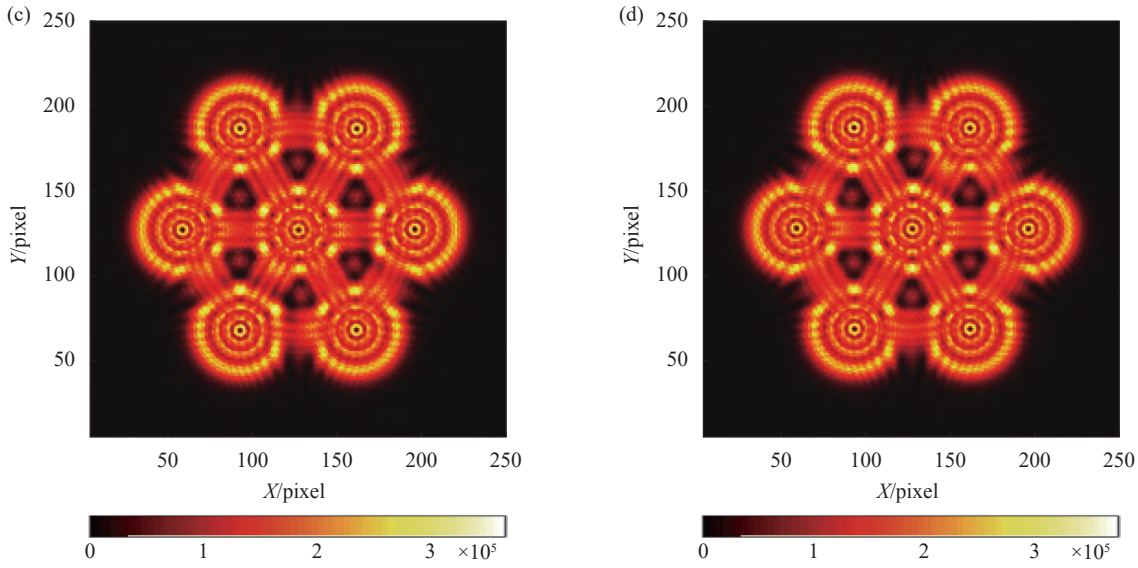


图 4 小幅值波前倾斜感知效果。(a) 倾斜波前；(b) 重建波前；(c) 焦前光强分布；(d) 焦后光强分布

Fig.4 Small amplitude wavefront tilt. (a) Tilt wavefront; (b) Reconstruction wavefront; (c) Intensity distribution intra-focus; (d) Intensity distribution extra-focus

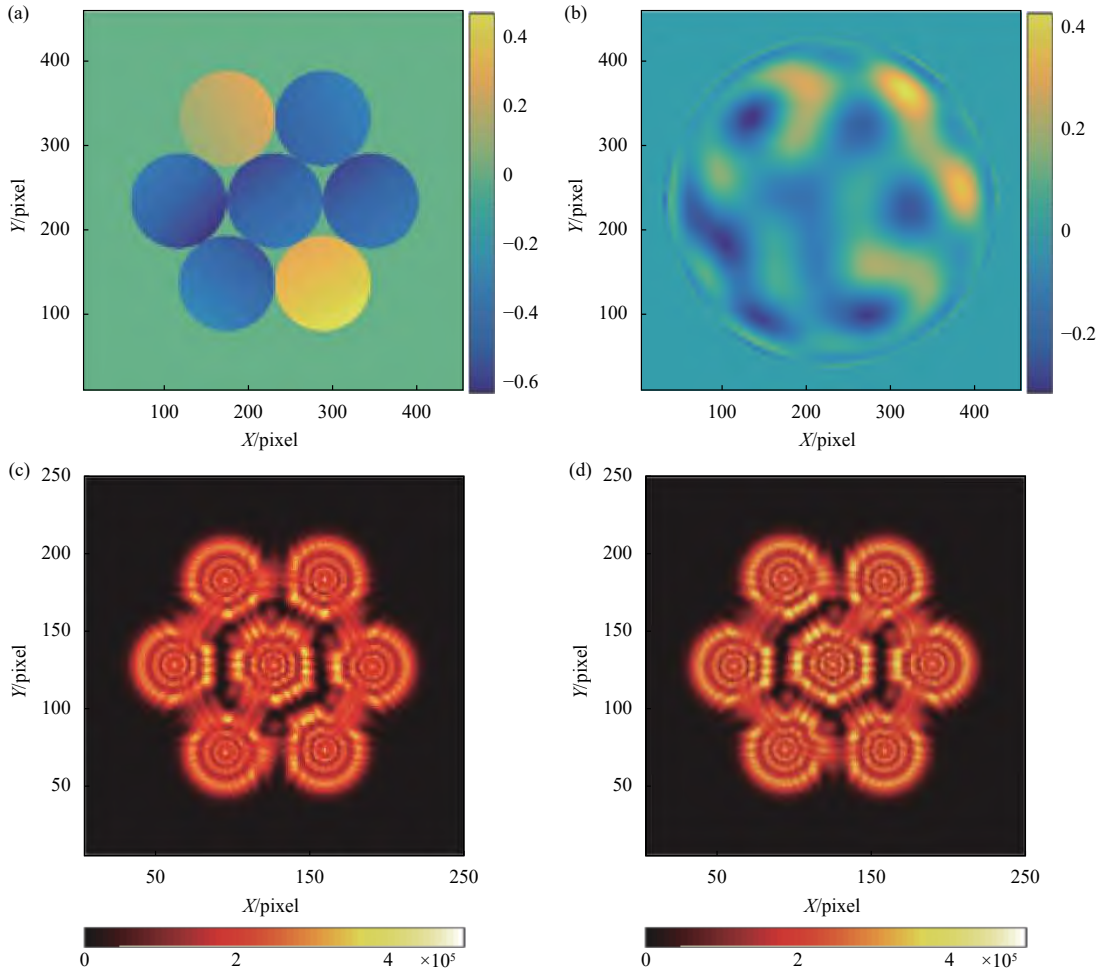


图 5 子镜整体低阶像差感知与调控。(a) 倾斜波前；(b) 重建波前；(c) 焦前光强分布；(d) 焦后光强分布

Fig.5 Perception and regulation of overall low order aberrations of sub mirror. (a) Tilt wavefront; (b) Reconstruction wavefront; (c) Intensity distribution intra-focus; (d) Intensity distribution extra-focus

## 3 可行性验证实验

利用分段式变形镜生成高阶波前像差，通过对波前倾斜的测试可验证曲率传感对边界异变的感知能力。利用变形镜波前倾斜解算验证平台如图 6 所示，采用激光光源经过扩束形成平行光并正入射到变形镜之上 (减少投射误差)，通过变形镜的调制形成波前倾斜，并通过曲率传感实现波前感知。通过分块变形镜面形的探测结果可以看出，该方法可实现整体趋势的准确感知 (前 11 阶 Zernike 多项式) 以及每块子镜之间由于倾斜所形成的波前突变。

利用变形镜对边界异变感知验证结果如图 7 所示，经过比较可得，所输入的变形 RMS 为 0.8$\lambda$($\lambda$=633 nm)，重建波前 RMS 为 0.7$\lambda$。利用低阶像差叠加高阶像差的模式验证了对波前倾斜的感知能力。

利用波前传感对具有倾斜的子镜进行闭环校正，波前倾斜解算相关系数如图 8 所示，闭环校正过程焦前焦后的光强差如图 9 所示。子镜的位姿由位于子镜底部的硬点控制 (共具有六个支腿) 与子镜广义位移量$\delta Q$(不局限于笛卡尔坐标表达) 的关系，因此平台雅可比矩阵可逆，故有：

$$\delta Q = J^{-1}\delta q \tag{2}$$

式中：$\delta q = [\delta L_{i2},\cdots,\delta L_{ij},\cdots,\delta L_{M6}]$；子镜倾斜维度空间多维雅可比矩阵为 $J = \begin{bmatrix} \dfrac{\partial Q_{1i}}{\partial q} & \dfrac{\partial Q_{2i}}{\partial q} \\ \vdots & \vdots \\ \dfrac{\partial Q_{1M}}{\partial q} & \dfrac{\partial Q_{2M}}{\partial q} \end{bmatrix}$。

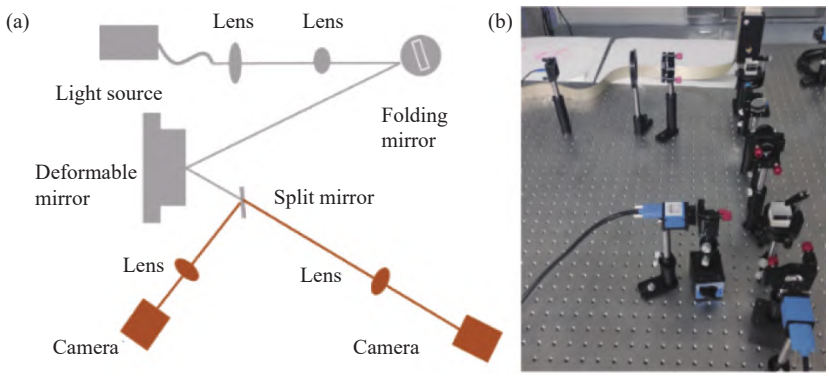


图 6 利用变形镜波前倾斜解算验证平台

Fig.6 Verification platform for wavefront tilt calculation using deformable mirror

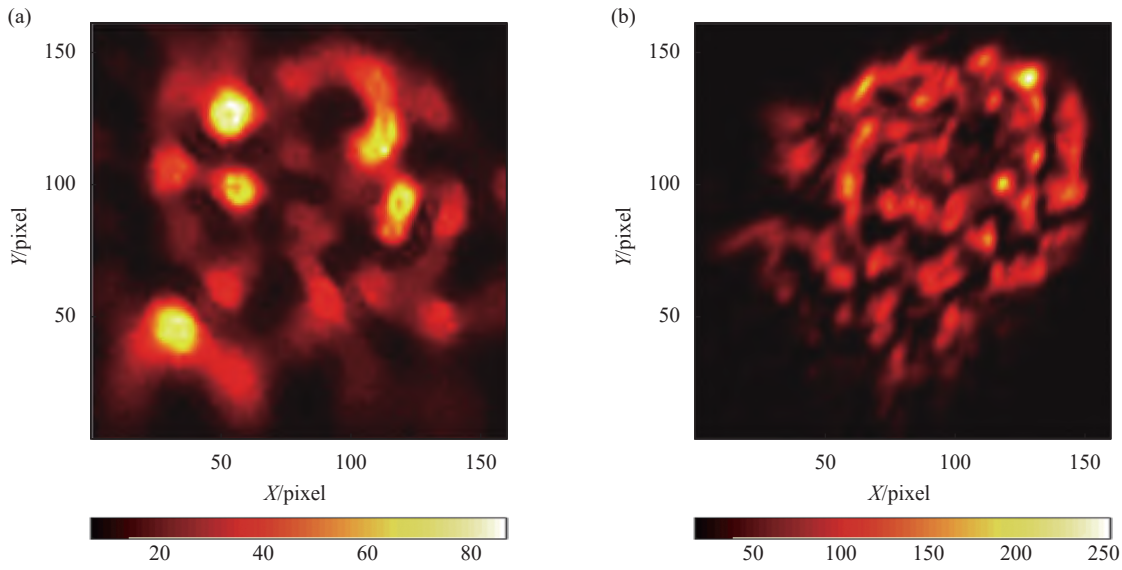

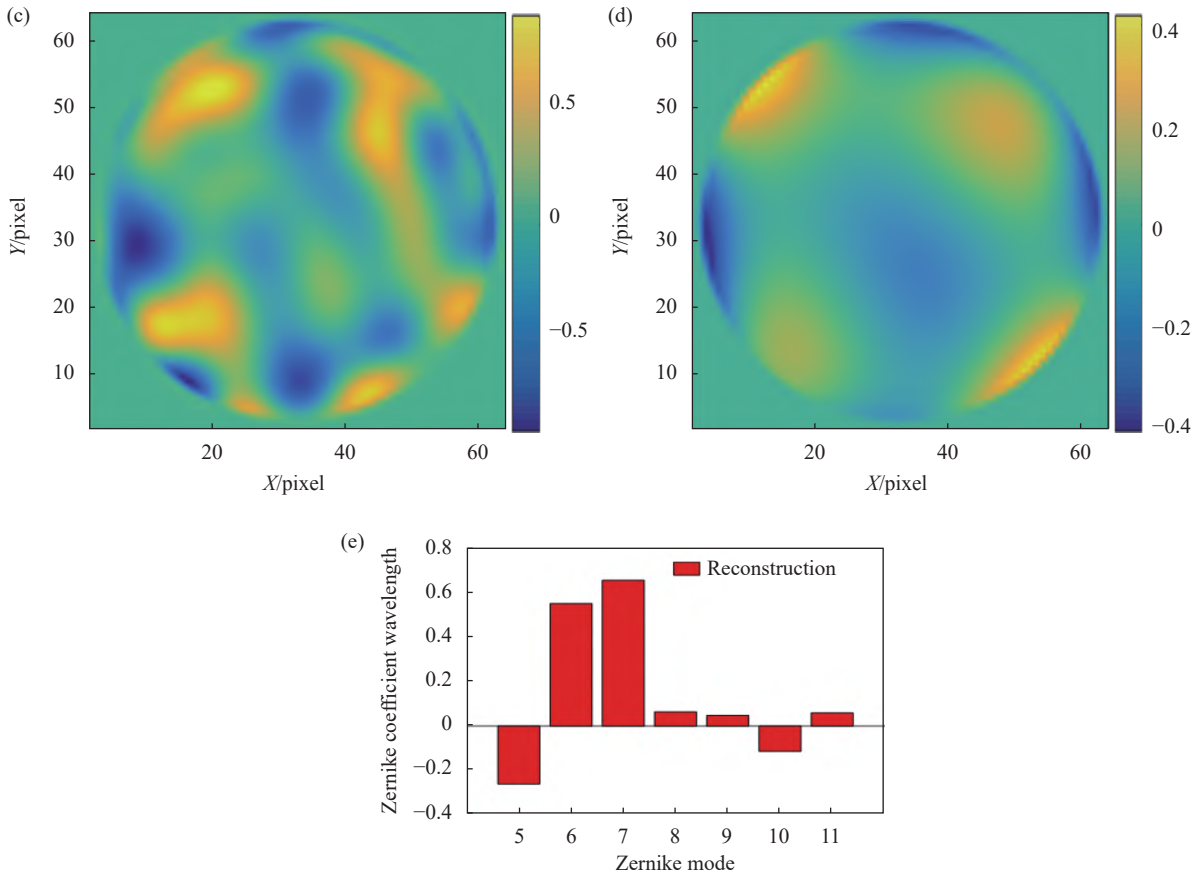


图 7 利用变形镜对边界异变感知验证结果。(a) 焦前光强分布; (b) 焦后光强分布; (c) 波前解算结果; (d) 低阶像差; (e) 低阶像差估计

Fig.7 Verification results of distortion perception of boundary using deformable mirror. (a) Intensity distribution intra-focus; (b) Intensity distribution extra-focus; (c) Wavefront solution results; (d) Low order aberration; (e) Low order aberration estimation

利用波前传感所获得的倾斜分量, 结合像差空间与镜面空间的映射关系可反解获得硬点的驱动量。在该分析中, 假设系统共有七块主镜, 每块子镜均存在倾斜误差, 利用焦前焦后的光强差实现波前传感, 并在此基础上实现闭环校正。结合图 3 和图 4 可得, 总调节范围大于 20$\lambda$。

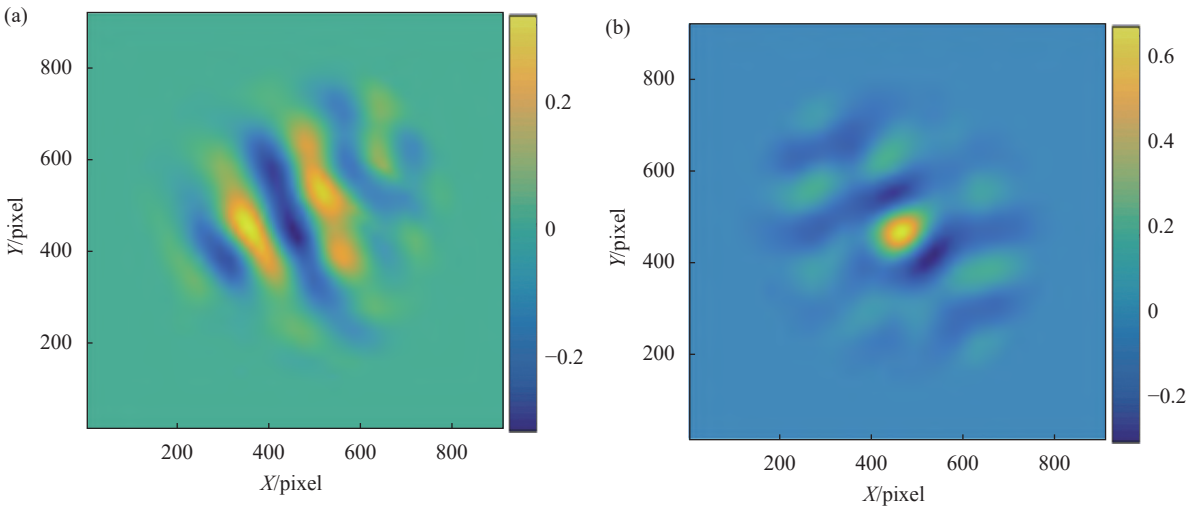

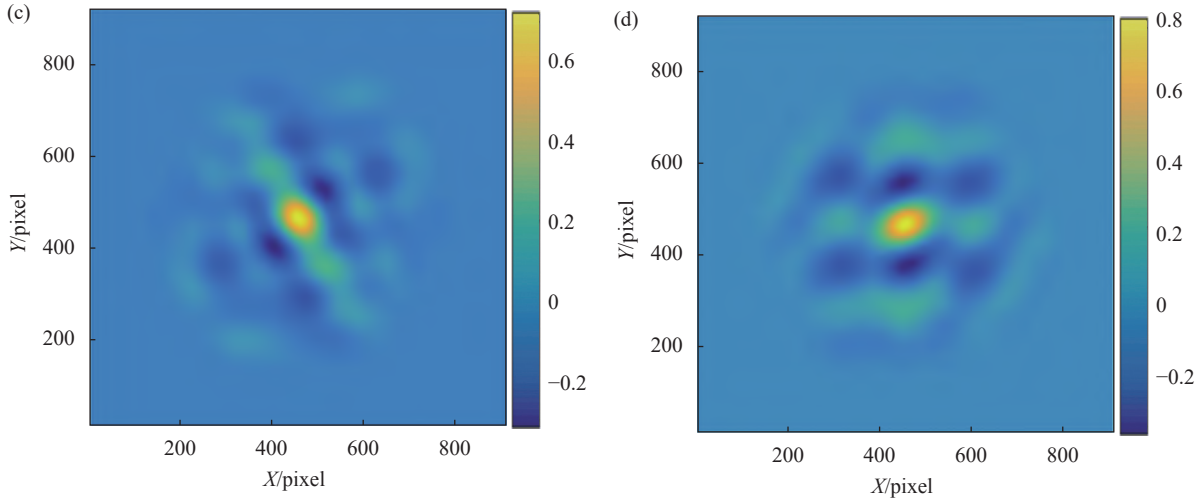


图 8 波前倾斜解算相关系数。(a) 初始情况; (b) 第一次修正; (c) 第二次修正; (d) 第三次修正

Fig.8 Correlation coefficient of wavefront tilt solution. (a) Initial condition; (b) First correction; (c) Second correction; (d) Third correction

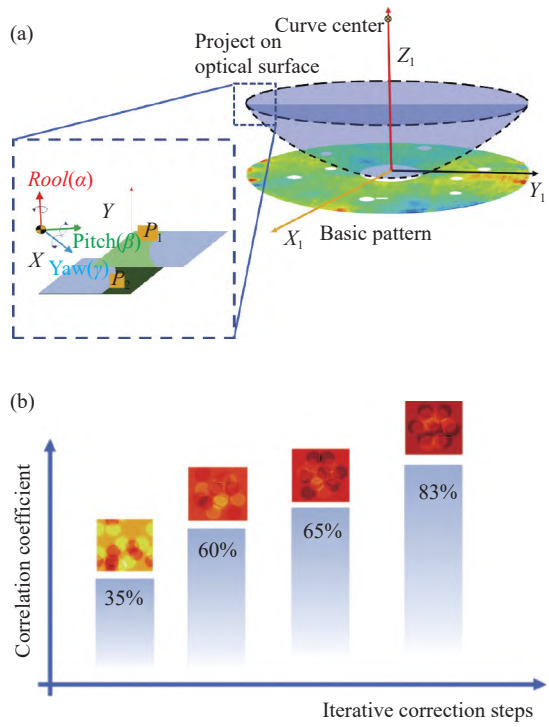


图 9 闭环校正过程。(a) 系统示意图; (b) 焦前焦后的光强差

Fig.9 Closed loop correction process. (a) System diagram; (b) Optical intensity difference before and after focus

## 4 结 论

大口径稀疏孔径望远镜是未来望远镜向 30 m 级发展的重要技术路线，其中系统共焦及其稳定性保持是实现大口径望远镜高质量成像、逼近设计理论极限的重要路径。利用曲率传感方法非干涉、大范围、波段鲁棒的特点，实现大口径稀疏孔径望远镜的共焦测量。在该分析中，假设系统共有七块主镜，每块子镜均存在倾斜误差，利用焦前焦后的光强差。最终，波前倾斜探测结果相关性高于 0.83，测量精度优于 0.2$\lambda$。利用曲率传感可克服多次移动标校以及逐个调节的缺点，实现了大通量的共焦误差感知与快速调控，为未来大口径稀疏孔径望远镜的建设打下技术基础。

**参考文献：**

[1] Fan Wenqiang, Wang Zhichen, Chen Baogang, et al. Review of the active control technology of large aperture ground telescopes with segmented mirrors [J]. ***Chinese Optics***, 2020, 13(6): 1194-1208. (in Chinese)

[2] Quirós-Pacheco F, Dam M , Bouchez A H , et al. The Giant Magellan Telescope natural guidestar adaptive optics mode: improving the robustness of segment piston control [C]//Proceedings of SPIE-Adaptive Optics Systems VIII, 2022, 12185: 1218517.

[3] Fanson J, Bernstein R, Ashby D, et al. Overview and status of the Giant Magellan Telescope project [C]//Proceedings of SPIE-Ground-based and Airborne Telescopes IX, 2020, 11445: 114451F.

[4] Bouchez A H, Conan R, Demers R T, et al. Overview and status of the GMT wavefront control system [C]//Proceedings of SPIE-Adaptive Optics Systems VIII, 2022, 12185: 121851C.

[5] Sitarski B N, Rakich A, Chiquito H, et al. The GMT telescope metrology system design [C]//Proceedings of SPIE-Astronomical Telescopes+Instrumentation, 2022, 12182: 1218207.

[6] Dovillaire G, Pierot D. Alignment and qualification of the Gaia telescope using a Shack-Hartmann sensor [C]//International Conference on Space Optics, 2016, 10562: 105625Y.

[7] Sabelhaus P A, Decker J E. An overview of the James Webb Space Telescope (JWST) project[C]//Optical, Infrared, and Millimeter Space Telescopes, SPIE, 2004, 5487: 550-563.

[8] Wang B, Dai Y, Jin Z, et al. Active maintenance of a segmented mirror based on edge and tip sensing [J]. ***Applied Optics***, 2021, 60(24): 7421-7431.

[9] Bai Xiaoquan, Guo Liang, Ma Hongcai, et al. Aberration coupling characteristics of axial and lateral misalignments of off-axis three-mirror telescopes [J]. ***Chinese Optics***, 2022, 15(4): 747-760. (in Chinese)

[10] McLeod B, Bouchez A H, Catropa D, et al. The wide field phasing testbed for the Giant Magellan Telescope [C]// Proceedings of SPIE-Ground-based and Airborne Telescopes IX, 2022, 12182: 1218208.

[11] Conan R, Lardière O, Herriot G, et al. The TMT/NFIRAOS LGS wavefront sensing demonstration bench [C]//1st AO4ELT Conference-Adaptive Optics for Extremely Large Telescopes, 2010: 05012.

[12] Fusco T, Meimon S, Clenet Y, et al. ATLAS: the E-ELT laser tomographic adaptive optics system [C]//Proceedings of SPIE-The International Society for Optical Engineering, 2010, 7736: 77360D.

[13] An Qichang, Wu Xiaoxia, Zhang Jingxu, et al. Large dynamic range curvature sensing for large-aperture active-optics survey telescope [J]. ***Infrared and Laser Engineering***, 2021, 50(10): 20210224. (in Chinese)

[14] Beichman C A, Rieke M, Eisenstein D, et al. Science opportunities with the near-IR camera (NIRCam) on the James Webb Space Telescope (JWST) [C]//Proceedings of SPIE-Astronomical Telescopes+Instrumentation, 2012, 8442: 84422N.

# Research on the method of co-focus detection for sparse aperture telescope based on curvature sensing

An Qichang[1,2], Wu Xiaoxia[1,2], Li Hongwen[1,2]

(1. . Changchun Institute of Optics, Fine Mechanics and Physics, Chinese Academy of Sciences, Changchun 130033, China;
2. Jilin Provincial Key Laboratory of Intelligent Wavefront Sensing and Control, Changchun 130033, China)

**Abstract:**

**Objective** For larger light collection area and detection sensitivity, the aperture of future telescopes is becoming larger and larger. The large sparse aperture telescope is one of the important tools for the future astronomy. Currently, the largest sparse aperture telescope is the Large Magellan Telescope (24 meters). For large sparse aperture telescopes, it is necessary to focus the direction of multiple sub mirrors on a single point, namely, co-focus. Co-focus (optical axis alignment) for sparse aperture is the foundation for achieving the established scientific goals of telescopes, and it is also the key to achieving functional synthesis of multi-channel systems. The dynamic range of wavefront sensing required for relatively large co-focus detection. For Hartmann sensors, a large sub aperture can be used to enhance the dynamic range, but it can lead to the addition of other aberration components in the sub aperture, deviating from the Gaussian assumption. For application scenarios such as fine astronomical observation, there will be huge limitations. At the same time, an excessive dynamic range can exacerbate the nonlinearity of the solution, leading to control degradation of the wavefront correction system.

**Methods** The co-focus measurement of large sparse aperture telescopes is mainly divided into two methods of using the focal plane and the pupil plane. Here, we first obtain two defocused star point images before and after focusing, and calculate the wavefront based on the wavefront curvature sensing method through the defocused star donut image. Afterwards, a mask is used to suppress the edge noise of the star image, which involves physical constraining. Then, co-focus perception and regulation can be achieved through plane fitting. The co-focus

detection method for sparse aperture telescopes based on curvature sensing is shown (Fig.2), which overcomes the disadvantage of traditional methods where light points overlap and are lost, requiring recalibration.

**Results and Discussions** By using segmented deformable mirrors to generate higher-order wavefront aberrations, the ability of curvature sensing to perceive boundary anomalies can be verified through testing the wavefront tilt. The verification platform for wavefront tilt calculation using deformable mirrors is shown (Fig.6). By utilizing the tilt component obtained from wavefront sensing, combined with the mapping relationship between aberration space and mirror space, the driving force of hard points can be obtained through inverse solution. In this analysis, it is assumed that the system has a total of 7 primary mirrors, each with tilt errors. By utilizing the difference in light intensity before and after focus plan, wavefront sensing is achieved, and closed-loop correction is achieved based on this. According to Fig.3 and Fig.4, the total adjustment range is greater than 20 wavelengths.

**Conclusions** By utilizing the non-interference, wide range, and band robustness characteristics of curvature sensing, co-focus measurement of large sparse aperture telescopes is achieved. This method can achieve parallel perception and control of multiple mirror tilts without performing focus recognition. In this analysis, it is assumed that the system has a total of 7 primary mirrors, and each sub mirror has tilt errors, utilizing the difference in light intensity before and after focusing. Finally, the correlation between the wavefront tilt detection results is higher than 0.83, and the measurement accuracy is better than 0.2$\lambda$ ($\lambda$=633 nm). By utilizing curvature sensing, the drawbacks of multiple moving calibrations and individual adjustments can be overcome. High throughput co-focus error perception and rapid regulation are realized. The method in this paper lays a technical foundation for the construction of future large aperture sparse aperture telescopes.

**Key words:** curvature sensing; wavefront aberration; sparse aperture telescope; co-focus

**Funding projects:** National Natural Science Foundation of China (12133009, 12373090); Youth Innovation Promotion Association of the Chinese Academy of Sciences (2020221); Chinese Academy of Sciences Key Project (YZQT024)